Available online at www.sciencedirect.com
SCIENCE DIRECT®
Journal of Molecular Spectroscopy 234 (2005) 84–92
Journal of MOLECULAR SPECTROSCOPY
www.elsevier.com/locate/jms

Absolute line intensities of $^{13}C^{16}O_2$ in the 4200–8500 cm^{-1} region

L. Wang [a,b], V.I. Perevalov [a,c], S.A. Tashkun [a,c], Y. Ding [a,b], S.-M. Hu [a,b,*]

[a] *USTC-Shanghai Institute for Advanced Studies, University of Science and Technology of China, Shanghai 201315, China*
[b] *Hefei National Laboratory for Physical Sciences at Microscale, Department of Chemical Physics, University of Science and Technology of China, Hefei 230026, China*
[c] *Laboratory of Theoretical Spectroscopy, Institute of Atmospheric Optics SB RAS, 1, Akademicheskii av., 634055 Tomsk, Russia*

Received 8 June 2005; in revised form 5 August 2005
Available online 7 October 2005

Abstract

The absolute line intensities of $^{13}C^{16}O_2$ were retrieved from Fourier-transform spectra recorded in the region 4200–8500 cm^{-1}. The accuracy of the line intensity determination is estimated to be 5% or better for most lines and about 10% for weak ones. The vibrational transition dipole moments squared and Herman–Wallis coefficients have been determined. The global fittings of the observed line intensities within the framework of the effective operators approach have been performed. As the result of the fittings, most line intensities are reproduced within the experimental accuracy. The comparison between the new measured data and the HITRAN database are also carried out.

Keywords: Carbon dioxide; Infrared; Fourier transform spectroscopy; Absolute line intensities; Transition dipole moment; Global modeling

1. Introduction

The infrared absorption spectroscopy of carbon dioxide is of the great interest for many important applications. One of them is the investigation of the greenhouse effect. Carbon dioxide is the second most important greenhouse gas after the water vapor. The increasing amount of carbon dioxide in the atmosphere enhances the greenhouse effect, blocking heat from escaping into the space and contributing to the warming of Earth's lower atmosphere. There are a lot of publications devoted to the infrared spectroscopy of this molecule but the majority of them deal with the principle isotopic species or with the line positions but not with the line intensities of the less abundant isotopic species. Compared to the line positions, the line intensities, especially the absolute intensities, are absent in the majority of the spectral regions for the less abundant isotopic species. But many applications like the study of the carbon dioxide impact on climate change and environment need these line intensities.

In this paper, we focus on $^{13}C^{16}O_2$, the second abundant species after $^{12}C^{16}O_2$ of the carbon dioxide molecule. The high-resolution absorption spectra of this isotopologue have been extensively studied during the last few decades. But the majority of the publications deal with the measurements of the line positions [1–27] and only few papers are devoted to the line intensity measurements [14,16,17,20,28–36]. To the best of our knowledge there are no publications of the measured line intensities for $^{13}C^{16}O_2$ isotopologue in the region above 4000 cm^{-1}. To continue our efforts in the study of the high-resolution spectra of $^{13}C^{16}O_2$ [25], we have undertaken a systematical measurement of the absolute line intensities of this isotopic species using Fourier Transform spectroscopy.

2. Experimental details

The ^{13}C enriched carbon dioxide sample was purchased from Aldrich Chemical. The stated isotopic concentration is 99% of ^{13}C for carbon atom with less than 6% for ^{18}O for oxygen atom. Since the accurate isotopic concentration is essential in the absolute line intensity study, it was

* Corresponding author. Fax: +86 551 360 2969.
E-mail address: smhu@ustc.edu.cn (S.-M. Hu).

0022-2852/$ - see front matter © 2005 Elsevier Inc. All rights reserved.
doi:10.1016/j.jms.2005.08.008

Table 1
Experimental conditions in the measurements of the strong bands of $^{13}C^{16}O_2$

Wavenumber (cm^{-1})	Pressure (Pa)	Path length (m)	Temperature (K)	Resolution (cm^{-1})	Detector
4700–5025	44.8	15	295.4	0.005	InSb
—	50.2	15	295.8	0.005	InSb
—	93.2	15	296.8	0.005	InSb
6000–6300	1113	15	294.8	0.005	InSb
—	1807	15	296.6	0.005	InSb
—	2433	15	294.8	0.005	InSb
6300–6400	1967	51	294.6	0.008	InSb
—	2310	51	295.0	0.008	InSb
—	2480	51	294.6	0.008	InSb
6720–6800	180.9	51	294.7	0.008	InSb
—	389	15	294.8	0.007	InSb
—	484	15	294.6	0.007	InSb

studied by a photo-ionization mass spectroscopy (PIMS) experiment measured with a re-electron time-of-flight mass spectrometer in the photochemistry end-station of National Synchrotron Radiation Laboratory, Hefei. The abundance of $^{13}C^{16}O_2$ was determined at 98.5% with accuracy about 0.2%. The $^{12}C^{16}O^{17}O$ isotopologue concentration in this sample should be no more than 0.1% which was confirmed by the absorption spectrum in the m-ir region. The absorption spectra were recorded in the spectral range from 4000 to 9500 cm^{-1}, with a Bruker IFS 120HR Fourier-transform spectrometer (FTS) equipped with a path length adjustable multi-pass gas cell. The maximum optical path length is 105 m. A tungsten source, CaF_2 beam splitter were used in all experiments. The cell was operated at room temperature, stabilized by an air-conditioning system. The pressure was measured using two capacitance manometers of 200 Pa and 133 hPa full-scale range with an overall accuracy of 0.5%. Different band-pass optic filters were applied to improve the signal-to-noise ratio. Although in most high-resolution studies, especially for accurate line position measurements, usually no apodization function is applied, here we use the Blackmann–Harris 3 term (BH3T)[1] apodization function to speed up the line profile fitting procedure which will be introduced in the next section.

Because of the wide spectral range and the large variation of the absorption line intensities, different experimental conditions were used as listed in Tables 1 and 2. The experimental conditions listed in Table 1 are typically for the strong bands while the experimental condition listed in Table 2 are for the weak ones. Overview spectrum in the region of 4300–8300 cm^{-1} is presented in Fig. 1.

3. Retrieval line strengths data

To retrieve line intensity values, the line profiles were fitted with a non-linear least-squares procedure. A PC based program "Intwin" written in C++ was applied to obtain the line parameters from the profile fitting to the observed spectrum. Voigt profile was adopted for each line. The fitting spectral region is determined as several times of the line width. If several lines are overlapped or very close to each other, the fitting region will be automatically enlarged to include all these lines. The Levenberg–Marquardt algorithm was used in the least-squares fitting procedure to minimize the deviation between the observed and calculated spectrum. Line position, integral line absorbance, Gaussian, and Lorentzian widths of each line and a baseline (as a linear function of the wavenumber) can be obtained from the fitting procedure. The Gaussian widths can be fixed at the corresponding Doppler width.

As an example, Fig. 2 shows the fitting results of a well-isolated line at 6253.896 cm^{-1}. The scattered symbols on the top panel present the observed spectrum and the solid lines give the resulted spectrum from the profile fitting. The residuals are given in the lower panels of the same figure.

As the result of fitting, we obtained the integrated absorbance for each line. It should be proportional to the product of the sample partial pressure and the absorption path length ($P \times L$). In Fig. 3 this linear dependence is illustrated for the lines centered at 5513.46, 6756.16, 8095.15, 4489.97, and 4817.06 $^{-1}$. The line strength of each line was finally determined as the average of the results from different spectra.

In our measurements, the pressure uncertainty is about 1% and the error from the temperature fluctuation and absorption path length is about 0.5%. The fitting error is estimated to be around 3% or better for well-isolated lines. This error may mainly come from the uncertainty in the baseline determination. Including all these errors mentioned above, we estimated that the accuracy of our absolute line intensities should be 5% or better for most lines and can be up to 10% for very weak lines.

The absolute line intensities or integrated absorption coefficients per unit pressure $\tilde{S}(T)$, in $cm^{-2}\,atm^{-1}$ at measurement temperature T, were deduced from the integrated line absorbance I using the equation

$$\tilde{S}(T) = I/PL, \quad (1)$$

[1] BH3T (Blackman–Harris 3 term) function: $W(\Delta) = a_0 + a_1\cos(2\pi\Delta/\Delta_m) + a_2\cos(4\pi\Delta/\Delta_m)$, where $a_0 = 0.42323$, $a_1 = 0.49755$, $a_2 = 0.07922$, Δ_m is the maximum optical path difference.

Table 2
Experimental conditions in the measurements of the weak bands of $^{13}C^{16}O_2$

Wavenumber (cm^{-1})	Pressure (Pa)	Path length (m)	Temperature (K)	Resolution (cm^{-1})	Detector
4000–5500	175	87	293.1	0.015	InSb
—	1034	33	291.4	0.015	InSb
—	1034	87	291.9	0.015	InSb
—	3672	51	294.6	0.015	InSb
—	3672	87	293.1	0.015	InSb
5000–9000	1034	33	292.4	0.015	Ge
—	1034	87	291.7	0.015	Ge
—	3672	51	292.7	0.015	Ge
—	3672	87	294.9	0.015	Ge

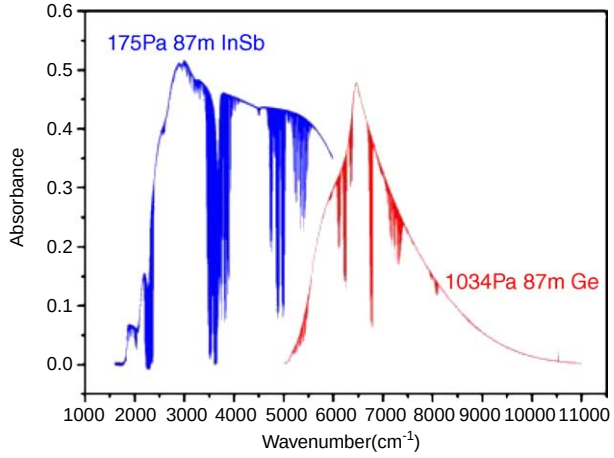

Fig. 1. Absorption spectrum of $^{13}C^{16}O_2$ in the 4300–8300 cm^{-1} region. The experimental conditions (gas pressure, path length, and used detector) are given. Many water lines appear in the regions of 5100–5500 and 7000–7400 cm^{-1}.

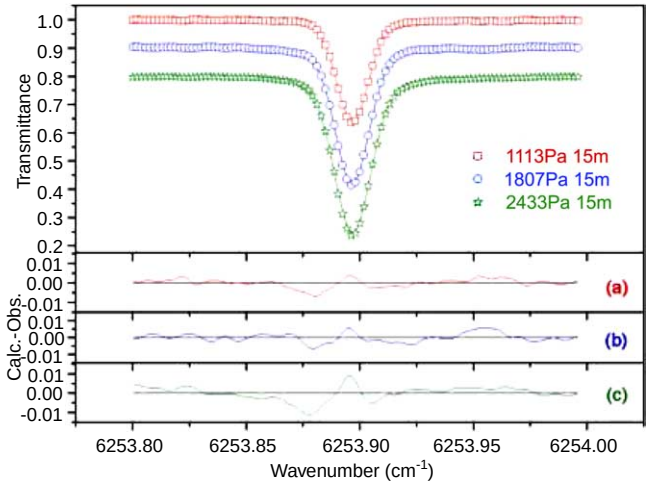

Fig. 2. Observed (in scattered symbols) and calculated (in solid lines) line profiles for the line $R(16)$ in the 30012–00001 band of $^{13}C^{16}O_2$ near 6253.896 cm^{-1} for different pressures and path lengths: (a) 1113 Pa, 15 m; (b) 1807 Pa, 15 m; (c) 2433 Pa, 15 m. Residuals are given in lower panels.

where P is the partial pressure of the studied isotopic species and L is the absorption path length. Then each $\tilde{S}(T)$ value was converted into the absorption line strength

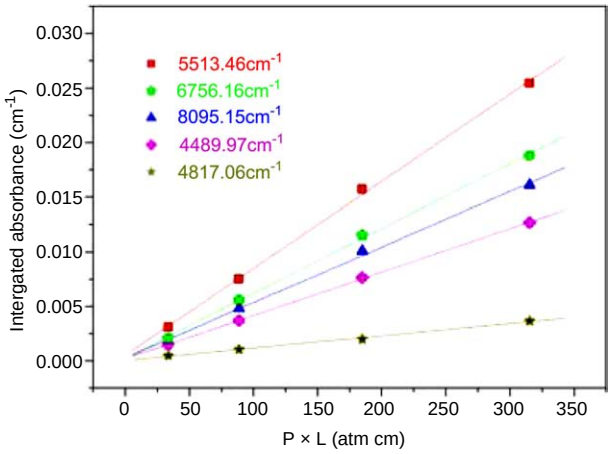

Fig. 3. Linear dependence of the integrated line absorbance on the product of sample pressure and absorption path length ($P \times L$).

$S(T_0)$, in $cm^{-1}/(molecule\ cm^{-2})$ at the standard temperature $T_0 = 296$ K, according to the following equation

$$S(T_0) = \frac{T}{273.15}\frac{1}{N_0}\frac{Q(T)}{Q(T_0)}\exp\left[\frac{hc}{k}E''\left(\frac{1}{T}-\frac{1}{T_0}\right)\right] \times \frac{1-\exp\left(-\frac{hc\,\nu_{N'J'\varepsilon'\leftarrow NJ\varepsilon}}{kT_0}\right)}{1-\exp\left(-\frac{hc\,\nu_{N'J'\varepsilon'\leftarrow NJ\varepsilon}}{kT}\right)}\tilde{S}(T), \quad (2)$$

where $N_0 = 2.68676 \times 10^{19}$ molecule cm^{-3} atm^{-1} is Loschmidt's number, h is Plank's constant, c is the speed of light in vacuum, k is the Boltzmann's constant, E'' (in cm^{-1}) is the energy of the lower ro-vibrational level of the transition and Q is the total partition function which can be retrieved according to [37]. The $S(T_0)$ values are given in the Supplementary Material.

4. Empirical data reduction

The absorption line strength $S_{N'J'\varepsilon'\leftarrow NJ\varepsilon}$ of the line corresponding to the transition $N'J'\varepsilon' \leftarrow NJ^{\varepsilon}$, where N and J are the vibrational index and rotational quantum number, respectively. And ε is the parity, which is related to the transition moment squared $W_{N'J'\varepsilon'\leftarrow NJ\varepsilon}$, in D^2 (1 Debye $= 3.33546 \times 10^{-30}$ C m), by the following equation:

$$S(T_0)=\frac{1}{4\pi\varepsilon_0}\frac{8\pi^3}{3hc}\frac{g_{N'J'\varepsilon'\leftarrow NJ\varepsilon}\nu_{N'J'\varepsilon'\leftarrow NJ\varepsilon}}{Q(T_0)}\times\exp\left(-\frac{hcE_{NJ\varepsilon}}{kT_0}\right)\left[1-\exp\left(-\frac{hc\nu_{N'J'\varepsilon\leftarrow NJ\varepsilon}}{kT_0}\right)\right]W_{N'J'\varepsilon\leftarrow NJ\varepsilon}, \quad (3)$$

where $\frac{1}{4\pi\varepsilon_0}=10^{-36}$ erg cm^3 D^{-2}, $\nu_{N'J'\varepsilon'\leftarrow NJ\varepsilon}$ is the line center in cm^{-1}, and $g_{NJ\varepsilon}$ is nuclear statistical weight of the lower level.

The transition moment squared can be presented as:

$$W_{N'J'\varepsilon\leftarrow NJ\varepsilon}=|R_{N'\varepsilon\leftarrow N\varepsilon}|^2L_{\Delta J}^{\Delta\ell_2}(J,\ell_2)(1+Am+Bm^2)^2, \quad (4)$$

where $|R_{N'\varepsilon\leftarrow N\varepsilon}|^2$ is the vibrational transition moment squared, $L_{\Delta J}^{\Delta\ell_2}(J,\ell_2)$ is the Hönl-London factor, m is equal to $J+1$ for R-branch lines and $-J$ for P-branch lines, A and B are the Herman–Wallis coefficients.

The Eqs. (3) and (4) were applied to retrieve the empirical data. The vibrational transition moment squared $|R_{N'\varepsilon\leftarrow N\varepsilon}|^2$ and Herman–Wallis coefficients A and B (when they are significant) were determined for each observed band by unweighted least-squares fitting to the experimental values of the transition moments squared $W_{N'J'\varepsilon'\leftarrow NJ\varepsilon}$. For this reason, Herman–Wallis coefficients A and B determined in this paper should be considered as the parameters reproducing the particular experimental data. These parameters are presented in Table 3 and the transition moment squared $W_{N'J'\varepsilon'\leftarrow NJ\varepsilon}$ determined for each line is presented in the Supplementary Material. In Fig. 4, two examples are given to show the dependence of the transition moment squared on the m values for the bands 30013–00001 and 31113–01101.

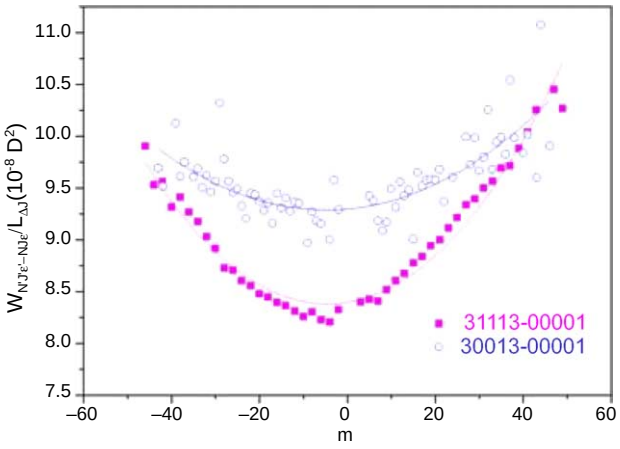

Fig. 4. Observed and calculated values $W_{N'J'\varepsilon'\leftarrow NJ\varepsilon}$ for the 30013–00001 and the hot band 31113–01101, divided by the corresponding Hönl-London factors $L_{\Delta J}^{\Delta\ell_2}$.

5. Modeling and fitting of the line intensities

5.1. Theoretical approach

Contrary to the empirical data reduction performed in the previous section, where each band is considered as an isolated band, in this section, we present the results of

Table 3
Summary of the experimental vibrational transition dipole moments squared $|R_{N'\varepsilon\leftarrow N\varepsilon}|^2$ in D^2 and the Herman–Wallis coefficients

Band center (cm^{-1})	Band	$\lvert R_{N'\varepsilon\leftarrow N\varepsilon}\rvert^2\times10^6$	$A\times10^4$	$B\times10^5$
4708.53	21113–01101ee	1.9925(43)		3.859(42)
	ff	1.9153(90)		4.147(46)
4748.06	20013–00001	1.43917(99)	2.113(96)	3.803(78)
4871.44	21112–01101ee	11.5980(48)		2.465(90)
	ff	11.7940(33)		1.881(77)
4887.38	20012–00001	12.48931(41)	1.800(54)	3.447(36)
4991.35	20011–00001	9.540(32)		
5013.78	21111–01101ee	9.203(63)		
	ff	9.248 (53)		
5168.60	01121–00001	0.019624(61)		
5951.60	30014–00001	0.0050417(37)	4.093(24)	4.940(81)
6088.21	31113–01101ee	0.09225(10)	2.508(7)	2.413(49)
	ff	0.092830(36)	2.099(77)	2.057(35)
6119.62	30013–00001	0.083731(87)	4.129(11)	4.668(73)
6241.97	30012–00001	0.211833(1)	3.247(47)	1.591(66)
6243.57	31112–01101ee	0.17223(27)	5.820(73)	1.092(43)
	ff	0.17299(41)	3.421(51)	0.263(65)
6363.62	30011–00001	0.04598(15)		
6397.55	31111–01101ee	0.051397(44)	5.67(15)	−1.367(44)
	ff	0.052104(20)	1.33(10)	−1.356(67)
6745.11	01131–01101ee	0.5589(26)		
	ff	0.5614(27)		
6780.21	00031–00001	0.6075(30)		
7481.57	40013–00001	0.00241930(87)	3.53(53)	0.991(68)
7600.12	40012–00001	0.0019105(84)	5.91(20)	−0.853(43)
7981.18	10032–00001	0.0070029(86)	1.633(58)	2.527(96)
8089.02	10031–00001	0.0217384(10)	1.032(42)	0.549(54)

The numbers in parentheses are one standard deviation in units of the last digit.

the simultaneous treatment of all bands lying in the same spectral region taking into account the resonance interactions between them in explicit form. In the case of the CO_2 molecule, vibrational states are grouped into polyads of the resonance interacting states due to the approximate relations between harmonic frequencies.

$$\omega_1 \approx 2\omega_2, \quad \omega_3 \approx 3\omega_2. \tag{5}$$

These polyads can be assigned with label P

$$P = 2V_1 + V_2 + 3V_3, \tag{6}$$

where V_i are vibrational quantum numbers.

Within the effective operators approach, the square of the transition dipole moment of vibration–rotation transition $P'N'J'\varepsilon' \leftarrow PNJ\varepsilon$ is given by [38–40]

$$W_{P'N'J'\varepsilon'\leftarrow PNJ\varepsilon} = (2J+1)\left| \sum_{V_1V_2\ell_2V_3} \sum_{\substack{2\Delta V_1+\Delta V_2+3\Delta V_3=\Delta P \\ \Delta\ell_2=0,\pm1,\pm2,\ldots}} {}^{J'}C^{V_1V_2\ell_2V_3}_{PN\varepsilon}\, {}^{J'}C^{V_1+\Delta V_1V_2+\Delta V_2\ell_2+\Delta\ell_2V_3+\Delta V_3}_{P'N'\varepsilon'} M^{|\Delta\ell_2|}_{\Delta V} \times\sqrt{f^{\Delta\ell_2}_{\Delta V}(V,\ell_2)(1+\delta_{\ell_2,0}+\delta_{\ell'_2,0}-2\delta_{\ell_2,0}\delta_{\ell'_2,0})}\; \Phi_{\Delta J,\Delta}\ell_2(J,\ell_2)\left(1+\sum_i \kappa^{\Delta V}_i V_i + F^{\Delta\ell_2}_{\Delta V}(J,\ell_2)\right)\right|^2. \tag{7}$$

Here, ${}^{J}C^{V_1V_2\ell_2V_3}_{PN\varepsilon}$ stands for the expansion coefficient determining the eigenfunction of the lower state

$$\Psi^{\mathrm{eff}}_{PNJ\varepsilon} = \sum_{\substack{2V_1+V_2+3V_3=P \\ \ell_2}} {}^{J}C^{V_1V_2\ell_2V_3}_{PN\varepsilon} |V_1V_2|\ell_2|V_3J\varepsilon\rangle. \tag{8}$$

The summation runs over all states within the polyad involved. The definition of the Wang-type basis functions $|V_1V_2|\ell_2|V_3\ J\ \varepsilon\rangle$ is given, for example, in [38]. In the same way, ${}^{J'}C^{V_1V_2\ell_2V_3}_{P'N'\varepsilon'}$ stands for the expansion coefficient within the upper-state polyad. The functions $\Phi_{\Delta J\Delta\ell_2}(J,\ell_2)$ for $\Delta\ell_2 = 0,\pm1$ coincide with the Clebsh–Gordon coefficients $(1\ \Delta\ell_2\ J\ell_2|\ (J+\Delta J)(\ell_2+\Delta\ell_2))$

$$\Phi_{\Delta J\Delta\ell_2}(J,\ell_2) = (1\ \Delta\ell_2\ J\ell_2|(J+\Delta J)(\ell_2+\Delta\ell_2)). \tag{9}$$

and the latter are related to the Hönl-London factors by the equation

$$|(1\ \Delta\ell_2\ J\ell_2|(J+\Delta J)(\ell_2+\Delta\ell_2))|^2 = \frac{L^{\Delta\ell_2}_{\Delta J}}{2J+1}. \tag{10}$$

The $f^{\Delta\ell_2}_{\Delta V}(V,\ell_2)$ functions are listed in Table 1 of [41] for small values of the quantum number differences V. The Herman–Wallis-type function $F^{\Delta\ell_2}_{\Delta V}(J,\ell_2)$ appearing in Eq. (7) can be written as

$$F^{\Delta\ell_2}_{\Delta V}(J,\ell_2) = b^{\Delta V}_J m + d^{\Delta V}_J\left[J(J+1)+m-\ell_2^2\right] \tag{11}$$

for the $\Delta\ell_2 = 0$ matrix elements,

$$F^{\Delta\ell_2}_{\Delta V}(J,\ell_2) = -\tfrac{1}{2}(b^{\Delta V}_J + 2a^{\Delta V}_K + d^{\Delta V}_{JQ})(2\ell_2\Delta\ell_2+1) + d^{\Delta V}_{JQ}\left[J(J+1)-\ell_2^2\right] \tag{12}$$

for the $\Delta J = 0$, $\Delta\ell_2 = \pm1$ matrix elements, and

$$F^{\Delta\ell_2}_{\Delta V}(J,\ell_2) = -\tfrac{1}{4}(d^{\Delta V}_{JQ} - d^{\Delta V}_J) - \tfrac{1}{2}(b^{\Delta V}_J + d^{\Delta V}_{JQ} + 2a^{\Delta V}_K) \times(2\ell_2\Delta\ell_2+1) - d^{\Delta V}_{JQ}\ell_2^2 + b^{\Delta V}_J m + d^{\Delta V}_J m^2 + (d^{\Delta V}_{JQ} - d^{\Delta V}_J)m(\ell_2\Delta\ell_2+\tfrac{1}{2}) \tag{13}$$

for $\Delta J = \pm1$, $\Delta\ell_2 = \pm1$ matrix elements.

The $M^{|\Delta\ell_2|}_{\Delta V}$, $\kappa^{\Delta V}_i$ $(i = 1,2,3)$, $a^{\Delta V}_K$, $b^{\Delta V}_J$, $d^{\Delta V}_J$, and $d^{\Delta V}_{JQ}$ parameters of the effective dipole moment matrix elements in Eqs. (7) and (11)–(13) describe simultaneously the strengths of all lines of cold and hot bands belonging to a series of transitions characterized by a given value of P.

5.2. Line intensities fitting

Using the approach described above, we performed the least-squares fittings of the line intensities measured in this paper. The measured bands belong to the three series of transitions: $\Delta P = 7$, 9, and 11. All measured bands are parallel bands, except of 01121–00001 band, which is a perpendicular one. The values of the expansion coefficients ${}^{J}C^{V_1V_2\ell_2V_3}_{PN\varepsilon}$ of the eigenfunctions have been obtained from the global fitting of the effective Hamiltonian parameters to the observed line positions in [26]. The partition functions $Q(T)$ and nuclear statistical weights are taken from [37].

The aim of the fitting procedure is to minimize the value of the dimensionless weighted standard deviation χ, defined according to the usual formula

$$\chi = \sqrt{\frac{\sum_{i=1}^{N}\left(\frac{S_i^{\mathrm{obs}} - S_i^{\mathrm{calc}}}{\delta_i}\right)^2}{(N-n)}}, \tag{14}$$

where S_i^{obs} and S_i^{calc} are, respectively, observed and calculated values of the intensity for the ith line; $\delta_i = \frac{S_i^{\mathrm{obs}}\sigma_i}{100\%}$, σ_i is the measurement error of the ith line in %, N is the number of fitted line intensities, and n is the number of adjusted parameters. To characterize the quality of a fit, it is sometimes more convenient to use the root mean square (RMS) deviation defined according to the equation

$$\mathrm{RMS} = \sqrt{\frac{\sum_{i=1}^{N}\left(\frac{S_i^{\mathrm{obs}} - S_i^{\mathrm{calc}}}{S_i^{\mathrm{obs}}}\right)^2}{N}} \times 100\%. \tag{15}$$

The third statistical characteristic, which is used in this paper, is the value of the mean residual (MR) for a given band. The MR is defined according to the equation

$$\mathrm{MR} = \frac{1}{N}\sum_{i=1}^{N}\frac{S_i^{\mathrm{obs}} - S_i^{\mathrm{calc}}}{S_i^{\mathrm{obs}}} \times 100\%, \tag{16}$$

where N is the number of fitted line intensities for a given band.

For the weighting, all the lines were divided into three groups: strong lines (line strength between 10^{-23} and 10^{-24} cm^{-1}/(molecule cm^{-2})), moderate lines (line strength between 10^{-24} and 10^{-25} cm^{-1}/(molecule cm^{-2})), and weak lines (line strength between 10^{-25} and 10^{-27} cm^{-1}/(molecule cm^{-2})). The weighting of the line intensities was done

Table 4
Summary of the line intensities fits

ΔP series	Number of lines	Number of bands	Number of branches	J_{max}	χ	RMS (%)	Number of adjusted parameters
7	504	7	15	62	0.67	3.5	8
9	524	9	19	55	0.73	3.5	7
11	172	4	8	53	0.64	3.2	4

Table 5
Band-by-band statistics of the fits

$P' \leftarrow P$		$V' \leftarrow V$		Br	J_{max}	N_{br}	RMS (%)	MR (%)
$\Delta P = 7$ series								
7	0	20011	00001	P	55	27	2.8	1.4
7	0	20011	00001	R	55	28	3.2	1.2
7	0	20012	00001	P	51	25	3.1	0.1
7	0	20012	00001	R	57	29	3.6	0.5
7	0	20013	00001	P	45	22	3.7	3.6
7	0	20013	00001	R	45	22	4.8	4.2
7	0	01121	00001	P	43	20	2.6	0.2
7	0	01121	00001	Q	47	23	2.0	−0.3
7	0	01121	00001	R	47	23	2.3	0.5
8	1	21111	01101	P	58	44	4.2	0.1
8	1	21111	01101	R	62	54	2.9	0.8
8	1	21112	01101	P	59	50	4.0	2.3
8	1	21112	01101	R	56	43	3.9	0.7
8	1	21113	01101	P	57	49	4.3	−1.5
8	1	21113	01101	R	55	46	2.8	−0.4
$\Delta P = 9$ series								
9	0	00031	00001	P	49	24	4.4	−1.5
9	0	00031	00001	R	47	23	1.7	1.2
9	0	30011	00001	P	37	18	2.7	1.4
9	0	30011	00001	R	43	21	4.0	1.2
9	0	30012	00001	P	55	27	5.2	2.1
9	0	30012	00001	R	49	25	3.7	1.2
9	0	30013	00001	P	45	22	3.9	2.4
9	0	30013	00001	R	43	22	3.9	2.8
9	0	30014	00001	P	39	19	1.7	−0.3
9	0	30014	00001	R	45	22	2.0	−1.3
10	1	0113	101101	P	53	47	3.2	0.8
10	1	0113	101101	Q	6	5	8.1	−7.5
10	1	0113	101101	R	37	33	2.3	0.3
10	1	31111	01101	P	40	30	3.0	1.2
10	1	31111	01101	R	40	35	3.6	2.5
10	1	31112	01101	P	49	38	3.2	−1.4
10	1	31112	01101	R	48	37	3.5	−1.0
10	1	31113	01101	P	44	38	3.4	1.9
10	1	31113	01101	R	46	38	3.2	0.0
$\Delta P = 11$ series								
11	0	10031	00001	P	53	26	2.5	0.0
11	0	10031	00001	R	53	23	3.0	0.1
11	0	10032	00001	P	43	21	2.9	−0.9
11	0	10032	00001	R	45	23	2.4	1.0
11	0	40012	00001	P	43	19	3.0	−1.3
11	0	40012	00001	R	41	19	4.2	1.5
11	0	40013	00001	P	41	20	3.4	−2.3
11	0	40013	00001	R	43	20	3.8	2.7

P' and P are numbers of upper and lower polyad, V' and V are upper and lower vibrational states according to HITRAN notation, Br is the branch identifier, J_{max} is the maximum value of the rotational quantum number in the file of observed data for a given branch, N_{br} is the number of the observed line intensities for a given branch, RMS (%) is the root mean squares of the residuals for a given branch (Eq. (15)), MR (%) is the mean value of the residuals for a given branch (Eq. (16)). See text for details.

according to assumed uncertainties σ_i which were set to 3% for the strong lines, 6% for the moderate lines, and 9% for the weak lines. These are the typical standard deviations of the line intensities measured at different experimental conditions (see Tables 1 and 2) for the respective groups of lines. The results of the least-squares fits for all three series of transitions are presented in Table 4. It can be seen that residuals of all fits are within the experimental accuracy. The RMS deviations corresponding to each branch and the values of MR are presented in Table 5. The sets of effective dipole moment parameters are given in Table 6. The residuals between the observed and calculated line strengths in all frequency regions are given in Fig. 5. This figure shows, although the residuals for the strongest lines are within the declared experimental accuracy about 5%, these lines have a tendency to be overestimated in the calculations. It could be several reasons for this. One of them is the non-linearity of detector and electronic acquisition set as it has been discussed in [41,42]. For example, in the case of [42] the measured non-linearity of the electronic acquisition set lead to up to 2% underestimation of the line strengths in the case of the strongest lines [42]. The non-linearity has not been investigated in the present work. Another reason could be in the weighting of the line intensities in the fit. We have performed the averaged estimates of the uncertainties of the line intensity determination for different groups of lines. But in fact, the uncertainties in the line intensity values can be very different for the individual lines.

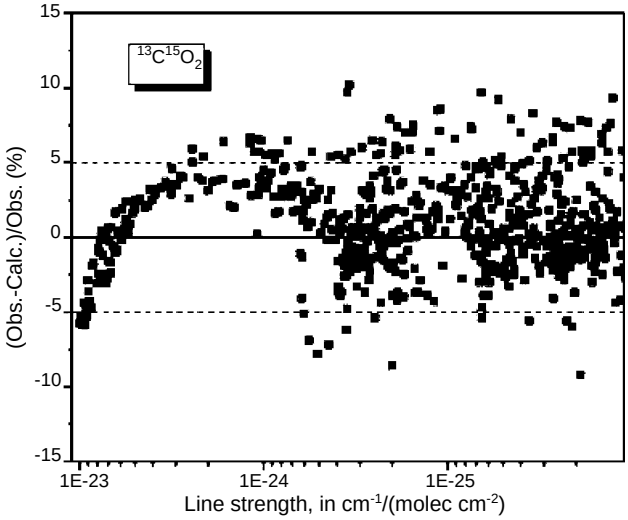

Fig. 5. Residuals between observed line strengths and those calculated within the framework of the method of effective operators. The line strengths values were converted for sample at natural isotopic abundance. Dash lines correspond to the estimated experimental accuracy.

The measured line intensities gave us the possibility to determine only two subsets of effective dipole moment parameters for each series of transitions: $\Delta V_3 = 1$ and $\Delta V_3 = 2$ subsets for the $\Delta P = 7$ series of transitions; $\Delta V_3 = 1$ and $\Delta V_3 = 3$ subsets for the $\Delta P = 9$ and $\Delta P = 11$ series of transitions. These subsets allow one to calculate the line intensities of all bands including

Table 6
Effective dipole moment parameters

Parameter[a]	ΔV_1	ΔV_2	ΔV_3	$\Delta \ell_2$	Value	Order
$\Delta P = 7$ series						
M	2	0	1	0	−0.34036(48)[b]	10^{-2}
κ_2	2	0	1	0	−0.211(15)	10^{-1}
b_J	2	0	1	0	0.127(29)	10^{-3}
d_J	2	0	1	0	0.162(11)	10^{-4}
M	1	2	1	0	0.2233(12)	10^{-3}
M	0	4	1	0	−0.998(27)	10^{-5}
M	0	1	2	1	−0.6977(24)	10^{-4}
b_J	0	1	2	1	−0.231(17)	10^{-2}
$\Delta P = 9$ series						
M	3	0	1	0	−0.24324(25)	10^{-3}
κ_2	3	0	1	0	−0.335(17)	10^{-1}
b_J	3	0	1	0	0.372(34)	10^{-3}
M	2	2	1	0	0.1738(11)	10^{-4}
M	1	4	1	0	−0.542(35)	10^{-6}
M	0	0	3	0	0.31653(47)	10^{-3}
κ_2	0	0	3	0	−0.435(30)	10^{-1}
$\Delta P = 11$ series						
M	1	0	3	0	0.6977(12)	10^{-4}
M	0	2	3	0	−0.1511(51)	10^{-5}
M	4	0	1	0	0.14134 (29)	10^{-4}
M	3	2	1	0	−0.698 (43)	10^{-6}

[a] The parameters M are given in *debye* while the other parameter are dimensionless. Only relative signs of M parameters within a given series of transitions are determined.

[b] The numbers in parentheses are one standard deviation in units of the last digit.

non-measured ones belonging to the respective $(\Delta P, \Delta V_3)$ sub-series of transitions. Because of the absence of the measured line intensities for the perpendicular bands belonging to $\Delta P = 9$ and $\Delta P = 11$ series, the parameters for the perpendicular bands in these series were not determined. So the sets of effective dipole moment parameters obtained in these cases do not give the possibility to generate the line intensities of the perpendicular bands, and the influence of Coriolis resonance interaction on the line intensities of the parallel bands can be taken into account only partly via the expansion coefficients of the eigenfunctions. Fortunately, the contributions to the line intensities of the parallel bands from the effective dipole moment parameters for the perpendicular bands are small even for strong resonance interactions.

In Table 6, we present only significant parameters from the point of view of our fits. For example, parameter $a_K^{\Delta V_1 - 0 \Delta V_2 - 1 \Delta V_3 - 2}$ is absent in this table because it was not significant in the respective fit.

6. Discussion and conclusion

In this paper, we present the first measurements of the absolute line intensities for the $^{13}C^{16}O_2$ isotopologue of carbon dioxide in the 4000–8500 cm^{-1} region. The existing in HITRAN database line intensity data for this isotopolgue in the above mentioned frequency region were obtained by means of DND calculations [43]. In Fig. 6, the comparison of DND calculated line intensities to our measured values is presented. There is an overall satisfactory agreement between DND calculated and measured values but for two bands 21113–01101 and 30014–00001 the residuals reach 20–29%. Our study considerably improves the $^{13}C^{16}O_2$ intensity data in 4000–8500 cm^{-1} region.

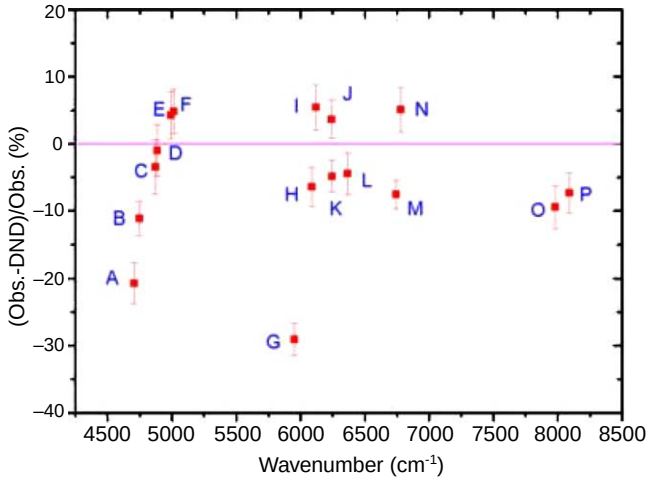

Fig. 6. Mean residuals between the line intensities observed in this paper and those presented in HITRAN database. (A) 21113–01101, (B) 20013–00001, (C) 21112–01101, (D) 20012–00001, (E) 20011–00001, (F) 21111–01101, (G) 30014–00001, (H) 31113–01101, (I) 30013–00001, (J) 30012–00001, (K) 31112–01101, (L) 30011–00001, (M) 01131–01101, (N) 00031–00001, (O) 10032–00001, and (P) 10031–00001.

Two approaches have been used for the modeling of the measured line intensities: approach based on the band intensity and Herman–Wallis factor and global approach based on the method of effective operators. The second approach is more preferable because it takes into account the resonance interactions between vibration–rotational states in an explicit way and allows one to predict the line intensities of the hot bands. Within the framework of this approach, we performed fittings of the effective dipole moment parameters to the observed line intensities. In all cases, the experimental accuracy was achieved. The fitted sets of the dipole moment parameters will be used to update end enlarge atmospheric CDSD-296 and high-temperature CDSD-1000 versions of the Carbon Dioxide Spectroscopic Databank [44].

Acknowledgments

The authors thank Dr. F. Qi in NSRL for the help in the isotope abundance determination with mass spectroscopy measurement. This work was jointly supported by the Natural Science Foundation of China (20103007, 20473079), by the Chinese Academy of Science, by the Russian Academy of Sciences within the framework of the program No. 2.10 "Optical Spectroscopy and Frequency Standards" and by Siberian Branch of Russian Academy of Sciences within the framework of the integration project 187 "Internet Accessible Information System: Spectral Properties of Hot Combustion Gases." The Foundation for Educational Development and Research of USTC-SIAS is also acknowledged.

Appendix A. Supplementary data

Supplementary data for this article are available on ScienceDirect (www.sciencedirect.com) and as part of the Ohio State University Molecular Spectroscopy Archives (http://msa.lib.ohio-state.edu/jmsa_hp.htm).

References

[1] J.Y. Mandin, J. Mol. Spectrosc. 67 (1977) 304–321.
[2] A. Baldacci, L. Linden, V. Malathy Devi, K. Narahari Rao, B. Fridovich, J. Mol. Spectrosc. 72 (1978) 135–142.
[3] C. Freed, L.C. Bradley, R.G. O'Donnell, IEEE J. Quantum Electron. 16 (1980) 1195–1206.
[4] G. Guelachvili, J. Mol. Spectrosc. 79 (1980) 72–83.
[5] R. Paso, J. Kauppinen, R. Anttila, J. Mol. Spectrosc. 79 (1980) 236–253.
[6] K.J. Siemsen, Opt. Commun. 34 (1980) 447–454.
[7] F.R. Petersen, J.S. Wells, A.G. Maki, K.J. Siemsen, Appl. Opt. 20 (1981) 3635–3640.
[8] A. Baldacci, C.P. Rinsland, M.A.H. Smith, K. Narahari Rao, J. Mol. Spectrosc. 94 (1982) 351–362.
[9] M.P. Esplin, R.J. Huppi, G.A. Vanasse, Appl. Opt. 21 (1982) 1681–1685.
[10] J. Kauppinen, K. Jolma, V.-M. Horneman, Appl. Opt. 21 (1982) 3332–3336.
[11] K. Jolma, J. Kauppinen, V.-M. Horneman, J. Mol. Spectrosc. 101 (1983) 300–305.

[12] D. Bailly, These, Universite de Paris-Sud, Paris, 1983.
[13] D. Bailly, C. Rossetti, J. Mol. Spectrosc. 105 (1984) 229–245.
[14] C.P. Rinsland, D.C. Benner, Appl. Opt. 23 (1984) 4523–4528.
[15] K. Jolma, J. Mol. Spectrosc. 111 (1985) 211–218.
[16] C.P. Rinsland, D.C. Benner, V. Malathy Devi, Appl. Opt. 24 (1985) 1644–1650.
[17] C.P. Rinsland, D.C. Benner, V. Malathy Devi, Appl. Opt. 25 (1986) 1204–1214.
[18] M.P. Esplin, L.S. Rothman, J. Mol. Spectrosc. 116 (1986) 351–363.
[19] M.P. Esplin, M.L. HokeHigh Resolution Fourier Transform Spectroscopy Technical Digest, vol. 21, OSA, Washington, DC, 1992, pp. 78–80.
[20] D.C. Benner, V. Malathy Devi, C.P. Rinsland, P.S. Ferry-Leeper, Appl. Opt. 27 (1988) 1588–1597.
[21] A.G. Maki, C.C. Chou, K.M. Evenson, L.R. Zink, J.T. Shy, J. Mol. Spectrosc 167 (1994) 211–224.
[22] S.A. Tashkun, V.I. Perevalov, J.-L. Teffo, M. Lecoutre, T.R. Huet, A. Campargue, D. Bailly, M.P. Esplin, J. Mol. Spectrosc. 200 (2000) 162–176.
[23] G. Weirauch, A. Campargue, J. Mol. Spectrosc. 207 (2001) 263–268.
[24] V. Malathy Devi, D.C. Benner, M.A.H. Smith, C.P. Rinsland, J. Quant. Spectrosc. Radiat. Transfer 76 (2003) 289–307.
[25] Y. Ding, V.I. Perevalov, S.A. Tashkun, J.-L. Teffo, A.W. Liu, S.M. Hu, J. Mol. Spectrosc. 222 (2003) 276–283.
[26] Y. Ding, P. Macko, D. Romanini, V.I. Perevalov, S.A. Tashkun, J.L. Teffo, S.M. Hu, A. Campargue, J. Mol. Spectrosc. 226 (2004) 146–160.
[27] Y. Ding, A. Campargue, E. Bertseva, S. Tashkun, V.I. Perevalov, J. Mol. Spectrosc. 231 (2005) 117–123.
[28] C.P. Rinsland, A. Baldacci, K. Narahari Rao, J. Mol. Spectrosc. 81 (1980) 256–261.
[29] J.W.C. Johns, J. Mol. Spectrosc. 125 (1987) 442–464.
[30] J.W.C. Johns, J. Mol. Spectrosc. 134 (1989) 433–439.
[31] J.W.C. Johns, J. Vander Auwera, J. Mol. Spectrosc. 140 (1990) 71–102.
[32] L. Rosenmann, S. Langlois, C. Delaye, J. Taine, J. Mol. Spectrosc. 149 (1991) 167–184.
[33] J.W.C. Johns, M. Noel, J. Mol. Spectrosc. 156 (1992) 403–414.
[34] J.W.C. Johns, J. Quant. Spectrosc. Radiat. Trans. 48 (1992) 572–576.
[35] J.-Y. Mandin, V. Dana, M. Badaoui, G. Guelachvili, M. Marillon-Chapey, Q. Kou, R.B. Wattson, L.S. Rothman, J. Mol. Spectrosc. 155 (1992) 393–402.
[36] L. Rosenmann, S. Langlois, J. Taine, J. Mol. Spectrosc. 158 (1993) 263–269.
[37] R.R. Gamache, R.L. Hawkins, L.S. Rothman, J. Mol. Spectrosc. 142 (1990) 205–219.
[38] V.I. Perevalov, E.I. Lobodenko, O.M. Lyulin, J.-L. Teffo, J. Mol. Spectrosc. 171 (1995) 435–452.
[39] J.-L. Teffo, O.M. Lyulin, V.I. Perevalov, E.I. Lobodenko, J. Mol. Spectrosc. 187 (1998) 28–41.
[40] S.A. Tashkun, V.I. Perevalov, J.L. Teffo, Vl.G. Tyuterev, J. Quant. Spectrosc. Radiat. Transfer. 62 (1998) 571–598.
[41] G. Guelachvili, Appl. Opt. 25 (1986) 4644.
[42] L. Regalia, X. Thomas, A. Hamdouni, A. Barbe, J. Quant. Spectrosc. Radiat. Transfer 57 (1997) 435–444.
[43] R.B. Wattson, L.S. Rothman, J. Quant. Spectrosc. Radiat. Transfer. 48 (1992) 763–780.
[44] S.A. Tashkun, V.I. Perevalov, J.L. Teffo, A.D. Bykov, N.N. Lavrentieva, J. Quant. Spectrosc. Radiat. Transfer 82 (2003) 165–196.